

THERMOELASTODYNAMIC CRACK ANALYSIS IN FUNCTIONALLY GRADED MATERIALS UNDER IMPACT LOADING

ALEXANDER V. EKHLAKOV^{1,3}, OKSANA M. KHAY², CHUANZENG ZHANG³,
JAN SLADEK⁴ AND VLADIMIR SLADEK⁴

¹Faculty of Architecture and Civil Engineering
RheinMain University of Applied Sciences
Kurt-Schumacher-Ring 18, D-65197 Wiesbaden, Germany
e-mail: alexander.ekhlakov@hs-rm.de

²Pidstryhach Institute for Applied Problems of Mechanics and Mathematics NASU
3b Naukova Str., 79060 Lviv, Ukraine
e-mail: khay@iapmm.lviv.ua

³Department of Civil Engineering
University of Siegen
Paul-Bonatz-Str. 9-11, D-57076 Siegen, Germany
e-mail: c.zhang@uni-siegen.de

⁴Institute of Construction and Architecture
Slovak Academy of Sciences
84503 Bratislava, Slovakia
e-mail: jan.sladek@savba.sk

Key Words: *Functionally Graded Materials, Boundary Element Method, Radial Integration Method, Dynamic Stress Intensity Factors.*

Abstract. A transient coupled thermoelastic analysis of two-dimensional, isotropic and linear elastic functionally graded materials under impact loading is investigated. For this purpose, a boundary element method is developed. Fundamental solutions of linear coupled thermoelasticity in Laplace-transformed domain for isotropic, homogeneous, and linear elastic solids are used for the boundary-domain integral equation formulation. The radial integration method is applied for the evaluation of the arising domain integrals. Numerical results for the dynamic stress intensity factors are presented and discussed.

1 INTRODUCTION

In recent years, functionally graded materials (FGMs) received considerable research interests in materials and engineering sciences. FGMs represent a new class of high-performance composite materials formed by continuously variable composition of the constituents over volume [1]. In comparison to the conventional composite materials, FGMs

possess many superior mechanical, thermal, corrosion-resistant and wear-resistant properties. FGMs can be widely applied in engineering structures and components such as electronic devices, blast protection, corrosion resistant coatings, wear-resistant coatings, thermal barrier coatings and biomaterials. As a representative example of FGMs, the ceramic/metal FGMs are compositionally graded from a ceramic phase to a metal phase. Ceramic/metal FGMs possess the desirable properties of metals such as high toughness, large mechanical strength and excellent bonding capability and high heat, wear and corrosion resistances of ceramics. An important application area of FGMs is their utilization in innovative engineering structures and structural elements under severe mechanical and thermal impact loading conditions. Because of the inherent brittle nature of ceramics, cracks or crack-like defects may develop in the manufacturing phase or during their services. Therefore, the fracture and damage analyses of FGMs under extreme mechanical and thermal impact loadings are of particular importance to their thermal and mechanical integrity, functionality, reliability and durability in engineering applications. Such analyses may provide a fundamental understanding of the failure mechanisms of FGMs that is helpful in the design, optimization and innovative applications of FGMs.

The initial-boundary value problems of transient linear coupled thermoelasticity are described by a system of coupled partial differential equations with variable coefficients supplemented by prescribed initial and boundary conditions. Due to the high mathematical complexity of the corresponding dynamic thermoelastic problems for non-homogeneous FGMs, analytical methods can be obtained only for very simple geometry and loading conditions. In general cases, numerical and experimental methods have to be applied to fracture and fatigue analyses in FGMs subjected to thermal and mechanical impact loadings.

In this paper, the two-dimensional (2-D) transient linear coupled thermoelastic crack problem in continuously non-homogeneous, isotropic and linear elastic FGMs under mechanical impact loading is investigated. The material properties of the FGMs are assumed to be continuous functions of the spatial coordinates, while Poisson's ratio is taken as constant. A boundary element method (BEM) is developed to analyze the responses of the crack with traction-free crack-faces. The transient linear coupled thermoelasticity is governed by the equations of motion and the thermal balance equation. The Laplace-transform technique is applied to eliminate the time-dependence in the governing equations. A boundary-domain integral representation is derived from the generalized Betti's reciprocal theorem by using the fundamental solutions for a homogeneous, isotropic and linear thermoelastic solid [2]. The boundary-domain integral equations (BDIEs) are obtained for mechanical and thermal field quantities [3-5]. Due to the material non-homogeneity, this approach leads to domain integrals involving the unknown quantities in addition to the conventional boundary integrals. The domain integrals are transformed into boundary integrals by using the radial integration method (RIM) [6,7]. A collocation method is implemented for the spatial discretization of the boundary-domain integral equations. After the boundary-domain integral equations have been solved numerically in the Laplace-transformed domain, the final time-dependent solutions are obtained by applying the inverse algorithm of Stehfest [8]. A displacement extrapolation technique is used to compute the dynamic stress intensity factors. Numerical examples for the dynamic stress intensity factors are presented and discussed to demonstrate the accuracy and the efficiency of the present BEM. The influences of the material gradation and the mechanical impact loading on the

dynamic stress intensity factors (SIFs) are investigated in details.

2 BOUNDARY-DOMAIN INTEGRAL EQUATIONS

Let us consider a continuously non-homogeneous, isotropic and linear elastic FGM in a 2-D domain. The material parameters such as the mass density $\rho(\mathbf{x})$, the Young's modulus $E(\mathbf{x})$, the thermal conductivity $k(\mathbf{x})$, the specific heat $c(\mathbf{x})$, the linear expansion coefficient $\alpha(\mathbf{x})$, etc. are assumed to depend continuously on the Cartesian coordinates, while the Poisson's ratio ν is a constant. In this case, the elasticity tensor is expressed as

$$c_{ijkl}(\mathbf{x}) = c_{ijkl}^0 \mu(\mathbf{x}) \quad (1)$$

with

$$c_{ijkl}^0 = \frac{2\nu}{1-2\nu} \delta_{ij} \delta_{kl} + \delta_{ki} \delta_{lj} + \delta_{kj} \delta_{li} \quad \text{and} \quad \mu(\mathbf{x}) = \frac{E(\mathbf{x})}{2(1+\nu)},$$

where $\mu(\mathbf{x})$ is the shear modulus, δ_{ij} denotes the Kronecker symbol. In the absence of body forces and heat sources, the equations of motion and the generalized heat-conduction equation in transient coupled thermoelasticity are given by

$$\begin{aligned} \sigma_{ij,j}(\mathbf{x}, t) - \rho(\mathbf{x}) \ddot{u}_i(\mathbf{x}, t) &= 0, \\ \left[k(\mathbf{x}) \theta_{,i}(\mathbf{x}, t) \right]_{,i} - \rho(\mathbf{x}) c(\mathbf{x}) \dot{\theta}(\mathbf{x}, t) - \eta(\mathbf{x}) \dot{u}_{k,k}(\mathbf{x}, t) &= 0, \end{aligned} \quad (2)$$

where σ_{ij} is the stress tensor, $k(\mathbf{x})$ is the thermal conductivity, $\eta = \gamma T_0 / k$ and T_0 is the reference temperature. Unless otherwise stated, the conventional summation rule over double indices is implied, a comma after a quantity indicates spatial derivatives, a dot over a quantity denotes time derivative, and Latin indices take the values of 1 and 2. A measure of the thermo-mechanical coupling due to the dilatational term $\eta \dot{u}_{k,k}$ in Eq. (2) is defined by a dimensionless coupling parameter [2, 9]

$$\delta = \frac{(1+\nu)}{(1-\nu)(1-2\nu)} \frac{E \alpha^2 T_0}{\rho c}, \quad (3)$$

that equals zero for an uncoupled problem. Applying the Laplace-transform to the governing equations (2) and using the Duhamel-Neumann relations [2] yields

$$\begin{aligned} c_{ijkl}^0 \left(\mu \bar{u}_{k,lj} + \mu_{,j} \bar{u}_{k,l} \right) - \left(\gamma \bar{\theta}_{,i} + \gamma_{,i} \bar{\theta} \right) - \rho p^2 \bar{u}_i &= 0, \\ \bar{\theta}_{,ii} + \frac{k_{,i}}{k} \bar{\theta}_{,i} - \frac{p}{\kappa} \bar{\theta} - \eta p \bar{u}_{k,k} &= 0, \end{aligned} \quad (4)$$

where γ and κ are the stress-temperature modulus and the thermal diffusivity, p denotes the complex Laplace-transform parameter and the superimposed bar denotes the Laplace-transformed quantities.

Integral representations of the displacements and the temperature at an arbitrary point are derived from the generalized Betti's reciprocal theorem for FGMs by using the fundamental solutions of the Laplace-transformed linear coupled thermoelasticity for homogeneous materials [2]. By moving the observation point to the boundary $\mathbf{x} \in \Gamma$ or keeping it in the domain $\mathbf{x} \in \Omega$ the following system of BDIEs for the mechanical and thermal fields at the boundary and interior points is obtained as

$$\begin{aligned} \bar{u}_j(\mathbf{x}, p) + \int_{\Gamma} \left[\bar{u}_i(\mathbf{y}, p) \bar{T}_{ij}(\mathbf{x}, \mathbf{y}, p) - \frac{1}{\tilde{E}(\mathbf{y}) \tilde{\alpha}(\mathbf{y})} \bar{t}_i(\mathbf{y}, p) \bar{U}_{ij}(\mathbf{x}, \mathbf{y}, p) \right] d\Gamma_y \\ - \kappa_0 \int_{\Gamma} \left[\bar{\theta}(\mathbf{y}, p) \bar{Z}_j(\mathbf{x}, \mathbf{y}, p) - \frac{\tilde{k}(\mathbf{y})}{\tilde{E}(\mathbf{y}) \tilde{\alpha}(\mathbf{y})} \bar{q}(\mathbf{y}, p) \bar{U}_j(\mathbf{x}, \mathbf{y}, p) \right] d\Gamma_y - \bar{F}_j^{(u)}(\mathbf{x}, p) = 0, \end{aligned} \quad (5)$$

$$\begin{aligned} \bar{\theta}(\mathbf{x}, p) - \frac{\kappa_0 \eta_0 P}{\gamma_0} \int_{\Gamma} \left[\bar{u}_i(\mathbf{y}, p) \bar{T}_i(\mathbf{x}, \mathbf{y}, p) - \frac{1}{\tilde{E}(\mathbf{y}) \tilde{\alpha}(\mathbf{y})} \bar{t}_i(\mathbf{y}, p) \bar{U}_i(\mathbf{x}, \mathbf{y}, p) \right] d\Gamma_y \\ + \kappa_0 \int_{\Gamma} \left[\bar{\theta}(\mathbf{y}, p) \bar{F}(\mathbf{x}, \mathbf{y}, p) - \frac{\tilde{k}(\mathbf{y})}{\tilde{E}(\mathbf{y}) \tilde{\alpha}(\mathbf{y})} \bar{q}(\mathbf{y}, p) \bar{T}(\mathbf{x}, \mathbf{y}, p) \right] d\Gamma_y - \bar{F}^{(0)}(\mathbf{x}, p) = 0, \end{aligned} \quad (6)$$

where \mathbf{x} and \mathbf{y} represent the source and the observation points, $\bar{U}_{ij}(\mathbf{x}, \mathbf{y}, p)$, $\bar{U}_i(\mathbf{x}, \mathbf{y}, p)$, $\bar{T}(\mathbf{x}, \mathbf{y}, p)$, $\bar{T}_{ij}(\mathbf{x}, \mathbf{y}, p)$, $\bar{T}_i(\mathbf{x}, \mathbf{y}, p)$, $\bar{Z}_i(\mathbf{x}, \mathbf{y}, p)$ and $\bar{F}(\mathbf{x}, \mathbf{y}, p)$ are the fundamental solutions [2,4,5]; $\bar{t}_i(\mathbf{x}, p) = \bar{\sigma}_{ij}(\mathbf{x}, p) n_j(\mathbf{x})$ are the components of the traction vector, $\bar{q}(\mathbf{x}, p) = k(\mathbf{x}) \bar{\theta}_{,i}(\mathbf{x}, p) n_i(\mathbf{x})$ is the heat flux and n_i denotes the components of the outward unit normal vector. Here, a tilde denotes the ratio of the non-homogeneous quantity to the homogeneous quantity that is designated by a zero subscript. The functions $\bar{F}_j^{(u)}$ and $\bar{F}^{(0)}$ describe the material non-homogeneity, which completely vanish for a homogeneous solid, and are defined [4,5] as

$$\begin{aligned} \bar{F}_j^{(u)}(\mathbf{x}, p) = -p^2 \varrho_0 \int_{\Omega} \left(\frac{\tilde{\rho}}{\tilde{E} \tilde{\alpha}} - 1 \right) \bar{U}_{ij}(\mathbf{x}, \mathbf{y}, p) \bar{u}_i(\mathbf{y}, p) d\Omega_y \\ + \mu_0 \int_{\Omega} \left[\frac{2(1-\nu)}{1-2\nu} \frac{1}{\tilde{\alpha}} \left(\frac{\tilde{E}_{,j}}{\tilde{E}} + \frac{\tilde{\alpha}_{,j}}{\tilde{\alpha}} \right) \bar{U}_{ik}(\mathbf{x}, \mathbf{y}, p) \right. \\ \left. - \left(\frac{1}{\tilde{\alpha}} - 1 \right) \left(\frac{1}{1-2\nu} \bar{U}_{ij,k}(\mathbf{x}, \mathbf{y}, p) + \bar{U}_{kj,i}(\mathbf{x}, \mathbf{y}, p) \right) \right] \bar{u}_{i,k}(\mathbf{y}, p) d\Omega_y \\ + \int_{\Omega} \left[p \left(\frac{\tilde{\rho} \tilde{c}}{\tilde{E} \tilde{\alpha}} - 1 \right) \bar{U}_j(\mathbf{x}, \mathbf{y}, p) - \gamma_0 \left(\frac{\tilde{E}_{,j}}{\tilde{E}} + \frac{\tilde{\alpha}_{,j}}{\tilde{\alpha}} \right) \bar{U}_{kk}(\mathbf{x}, \mathbf{y}, p) \right] \bar{\theta}(\mathbf{y}, p) d\Omega_y \\ + \kappa_0 \int_{\Omega} \left[\left(\frac{\tilde{k}}{\tilde{E} \tilde{\alpha}} - 1 \right) \bar{U}_{j,i}(\mathbf{x}, \mathbf{y}, p) - \frac{1}{\eta_0} \frac{\tilde{k}}{\tilde{E} \tilde{\alpha}} \left(\frac{\tilde{E}_{,i}}{\tilde{E}} + \frac{\tilde{\alpha}_{,i}}{\tilde{\alpha}} \right) \bar{U}_j(\mathbf{x}, \mathbf{y}, p) \right] \bar{\theta}_{,i}(\mathbf{y}, p) d\Omega_y, \end{aligned} \quad (7)$$

$$\begin{aligned}
 \bar{F}^{(0)}(\mathbf{x}, p) = & \frac{\kappa_0 \eta_0 p}{\gamma_0} \left\{ p^2 \varrho_0 \int_{\Omega} \left(\frac{\tilde{\varrho}}{\tilde{E} \tilde{\alpha}} - 1 \right) \bar{U}_i(\mathbf{x}, \mathbf{y}, p) \bar{u}_i(\mathbf{y}, p) d\Omega_y \right. \\
 & + \mu_0 \int_{\Omega} \left[-\frac{2(1-\nu)}{1-2\nu} \frac{1}{\tilde{\alpha}} \left(\frac{\tilde{E}_{,j}}{\tilde{E}} + \frac{\tilde{\alpha}_{,j}}{\tilde{\alpha}} \right) \bar{U}_i(\mathbf{x}, \mathbf{y}, p) \right. \\
 & \quad \left. \left. + \left(\frac{1}{\tilde{\alpha}} - 1 \right) \left(\frac{1}{1-2\nu} \bar{U}_{i,j}(\mathbf{x}, \mathbf{y}, p) + \bar{U}_{j,i}(\mathbf{x}, \mathbf{y}, p) \right) \right] \bar{u}_{i,j}(\mathbf{y}, p) d\Omega_y \right\} \quad (8) \\
 & + p \int_{\Omega} \left[-\left(\frac{\tilde{\varrho} \tilde{c}}{\tilde{E} \tilde{\alpha}} - 1 \right) \bar{T}(\mathbf{x}, \mathbf{y}, p) + \kappa_0 \eta_0 \left(\frac{\tilde{E}_{,j}}{\tilde{E}} + \frac{\tilde{\alpha}_{,j}}{\tilde{\alpha}} \right) \bar{U}_j(\mathbf{x}, \mathbf{y}, p) \right] \bar{\theta}(\mathbf{y}, p) d\Omega_y \\
 & + \kappa_0 \int_{\Omega} \left[-\left(\frac{\tilde{k}}{\tilde{E} \tilde{\alpha}} - 1 \right) \bar{T}_{,i}(\mathbf{x}, \mathbf{y}, p) + \frac{1}{\eta_0} \frac{\tilde{k}}{\tilde{E} \tilde{\alpha}} \left(\frac{\tilde{E}_{,i}}{\tilde{E}} + \frac{\tilde{\alpha}_{,i}}{\tilde{\alpha}} \right) \bar{T}(\mathbf{x}, \mathbf{y}, p) \right] \bar{\theta}_{,i}(\mathbf{y}, p) d\Omega_y.
 \end{aligned}$$

The BDIEs (5) and (6) contain boundary and domain integrals with singular kernels. The strongly singular integrals are interpreted in the sense of the Cauchy principal value. Making use of the singularity subtraction technique and the variable transformation technique the strong and weak singularities in Eqs. (5) and (6) can be removed [10,4,5].

3 NUMERICAL SOLUTION PROCEDURE

In order to avoid the domain discretization into internal cells for evaluating the domain integrals in Eqs. (7) and (8) the radial integration method (RIM) developed by Gao is applied [6, 7]. The functions (7) and (8) can be rewritten in matrix form [5] as

$$\bar{\mathbf{F}}(\mathbf{x}, p) = \int_{\Gamma} \bar{\mathbf{F}}(\mathbf{x}, \mathbf{y}, p) \bar{\mathbf{u}}(\mathbf{y}, p) d\Gamma + \int_{\Omega} \mathbf{G}(\mathbf{x}, \mathbf{y}, p) \bar{\mathbf{u}}(\mathbf{y}, p) d\Omega, \quad (9)$$

where $\bar{\mathbf{F}}$ is the vector of functions $\bar{F}_i^{(u)}$ and $\bar{F}^{(0)}$, $\bar{\mathbf{u}}$ is the vector containing the displacements \bar{u}_i and the temperature $\bar{\theta}$, and the 3×3 matrices $\bar{\mathbf{F}}$ and \mathbf{G} are given in [5]. The unknown fields \bar{u}_i or $\bar{\theta}$ are approximated by a series of prescribed radial basis functions and the linear polynomials

$$\begin{aligned}
 \bar{u}_i(\mathbf{x}, p) = & \sum_A \bar{\alpha}_i^A(p) \phi^A(R) + \bar{a}_i^j(p) x_j + \bar{a}_i^0(p), \\
 \sum_{A=1} \bar{\alpha}_i^A(p) = & \sum_{A=1} \bar{\alpha}_i^A(p) x_j^A = 0,
 \end{aligned} \quad (10)$$

where $R = \|\mathbf{x} - \mathbf{x}^A\|$ is the distance from the application point A to the field point \mathbf{x} , $\bar{\alpha}_i^A$ and \bar{a}_i^j are the unknown expansion coefficients to be determined and x_j^A denotes the coordinates at the application point A , which consist of all boundary nodes and some selected internal nodes. The fourth order spline-type radial basis function [6, 7] is used

$$\phi^A(R) = 1 - 6R^2 + 8R^3 - 3R^4. \quad (11)$$

The unknown coefficients $\bar{\alpha}_i^A$ and \bar{a}_i^j can be determined by applying the application point A in Eq. (11) to every node. Then, a system of linear algebraic equations can be obtained in matrix form as

$$\{\bar{u}\} = [\Phi]\{\bar{\alpha}\}, \quad (12)$$

where $\{\bar{\alpha}\}$ is the vector consisting of the coefficients $\bar{\alpha}_i^A$ for all points and \bar{a}_i^j . If two application points do not coincide, the matrix $[\Phi]$ is invertible and thereby

$$\{\bar{\alpha}\} = [\Phi]^{-1}\{\bar{u}\}. \quad (13)$$

Substitution of Eqs. (10) into the domain integrals of Eq. (9) yields

$$\int_{\Omega} \bar{G}_{ij} \bar{u}_j d\Omega = \bar{\alpha}_j^a \int_{\Omega} \bar{G}_{ij} \phi^a d\Omega + \bar{a}_j^k \int_{\Omega} \bar{G}_{ij} y_k d\Omega + \bar{a}_j^0 \int_{\Omega} \bar{G}_{ij} d\Omega. \quad (14)$$

Applying the RIM [5-7] to the domain integrals in Eq. (14) results in

$$\int_{\Omega} \bar{G}_{ij} \bar{u}_j d\Omega = \bar{\alpha}_j^a \int_{\Gamma} \frac{1}{r} \frac{\partial r}{\partial n} \bar{F}_{ij}^a d\Gamma + \bar{a}_j^k \int_{\Gamma} \frac{r_{,k}}{r} \frac{\partial r}{\partial n} \bar{F}_{ij}^1 d\Gamma + (\bar{a}_j^k x_k + \bar{a}_j^0) \int_{\Gamma} \frac{1}{r} \frac{\partial r}{\partial n} \bar{F}_{ij}^0 d\Gamma \quad (15)$$

with the radial integrals

$$\bar{F}_{ij}^a = \int_0^r r \bar{G}_{ij} \phi^a dr, \quad \bar{F}_{ij}^1 = \int_0^r r^2 \bar{G}_{ij} dr, \quad \bar{F}_{ij}^0 = \int_0^r r \bar{G}_{ij} dr. \quad (16)$$

It is important to note here that the term $r_{,i}$ appearing in the radial integrals is constant [7] and the relation $y_k = x_k + r_{,k} r$ is used for the transformation from \mathbf{y} to \mathbf{r} . The radial integrals (16) are regular and can be evaluated numerically by using standard Gaussian quadrature for every field point.

The BDIEs (5) and (6) can be solved numerically by applying a collocation method. The usual discretization procedure applied in BEM is utilized for the boundary discretization of the BDIEs in the Laplace-transformed domain [2, 10]. After numerical integrations and imposing the prescribed boundary conditions the system of $3N$ linear algebraic equations can be written as

$$\begin{aligned} \mathbf{A}^b \mathbf{x}^b &= \mathbf{y}^b + \mathbf{D}^b \mathbf{u}, & \text{for boundary nodes,} \\ \mathbf{A}^i \mathbf{x}^b + \mathbf{u}^i &= \mathbf{y}^i + \mathbf{D}^i \mathbf{u}, & \text{for internal nodes,} \end{aligned} \quad (17)$$

where $N = N^w + N^d$ is the total number of the unknown quantities, N^w and N^d correspond to the number of the boundary nodes and the number of the internal nodes, respectively, the superscripts b and i denote the quantities at a boundary point and an interior point, respectively. In Eqs. (17), \mathbf{x}^b is the $3N^w$ vector of the unknown values of the displacements \bar{u}^i , the tractions \bar{t}_i , the temperature $\bar{\theta}$ and the heat flux \bar{q} at the boundary collocation points, \mathbf{u}^i is the $3N^d$ vector of the unknown displacements \bar{u}_i and the temperature $\bar{\theta}$ at the interior

collocation points, \mathbf{u} is the $3N$ vector composed of vectors \mathbf{x}^b and \mathbf{u}^i , \mathbf{y}^b and \mathbf{y}^i denote the $3N^w$ and $3N^d$ vectors of the prescribed boundary quantities. The sizes of the matrices \mathbf{A}^b , \mathbf{A}^i , \mathbf{D}^b and \mathbf{D}^i are $3N^w \times 3N^w$, $3N^d \times 3N^w$, $3N^w \times 3N$ and $3N^d \times 3N$, respectively. It should be noted that the matrices \mathbf{D}^b and \mathbf{D}^i stem from the evaluation of the domain integrals $\bar{F}_j^{(u)}$ and $\bar{F}^{(0)}$. The system of linear algebraic equations (17) is solved numerically to obtain the boundary unknowns \mathbf{x}^b and the primary interior field quantities \mathbf{u}^i for discrete values of the Laplace-transform parameter p . The final time-dependent solutions are found by the numerical inversion of the Laplace transform using the Stehfest's algorithm [8].

Different methods can be used for the evaluation of the SIFs. In this analysis, the extrapolation technique following directly from the asymptotic expansion of the displacements in the vicinity of the crack-tip is employed [10,11]. For a crack located on the x_1 -axis, the dynamic mode-I and mode-II SIFs are related to the crack-opening-displacements $\Delta u_i(\mathbf{x}, t)$ by

$$\begin{Bmatrix} K_I(t) \\ K_{II}(t) \end{Bmatrix} = \frac{\sqrt{2\pi}}{\kappa+1} \mu^{\text{tip}} \lim_{\varepsilon \rightarrow a} \frac{1}{\sqrt{a-\varepsilon}} \begin{Bmatrix} \Delta u_2(\varepsilon, t) \\ \Delta u_1(\varepsilon, t) \end{Bmatrix}, \quad (18)$$

where $\kappa = 3 - 4\nu_0$ or $\kappa = (3 - \nu_0)/(1 + \nu_0)$ for plane-strain or plane-stress conditions, respectively, μ^{tip} is the shear modulus at the crack-tip, and ε is a small distance from the crack-tip to the considered node on the crack-faces.

4 NUMERICAL RESULTS

As a numerical example we consider an edge crack in a rectangular, isotropic and linear thermoelastic FG/homogeneous bimaterial plate, which is subjected to impact loading $\sigma(\mathbf{x}, t) = \sigma_0 H(t)$ as shown in Fig. 1a. Here, σ_0 is the constant loading amplitude and $H(t)$ is the Heaviside step function. The geometry of the cracked plate is determined by the width $w = 1$,

height $2h = 3w$ and crack-length $a = 0.4w$. An exponential material gradation with the gradient parameter α_g in the x_2 -direction perpendicular to the crack-line of the FG coated structure is assumed as [5]

$$E = E_0 \exp(\alpha_g x_2), \quad k = k_0 \exp(\alpha_g x_2), \quad c = c_0 \exp(\alpha_g x_2). \quad (19)$$

The mass density, the Poisson's ratio and the linear thermal expansion coefficient are taken as $\rho(\mathbf{x}) = 1$, $\alpha(\mathbf{x}) = 0.02$ and $\nu = 0.25$, respectively. Plane-strain condition is assumed in the numerical calculations. The sub-domain technique is adopted in crack analysis [11]. The plate is virtually divided into two sub-domains along the crack-line, and the fictitious boundary is shown on Fig. 1b as dot-dashed line. The non-homogeneity of the FG layer induces a mixed mode crack-tip loading even though the cracked plate is subjected to a pure tensile loading on the top and the bottom side symmetric to the crack-faces, i.e., the mode-II dynamic SIF is also

present along with the mode-I dynamic SIF. For convenience, the dynamic SIFs are normalized as $\bar{K}_{I,II}(t) = K_{I,II}(t) / K^*$ with $K^* = \sigma_0 \sqrt{\pi a}$.

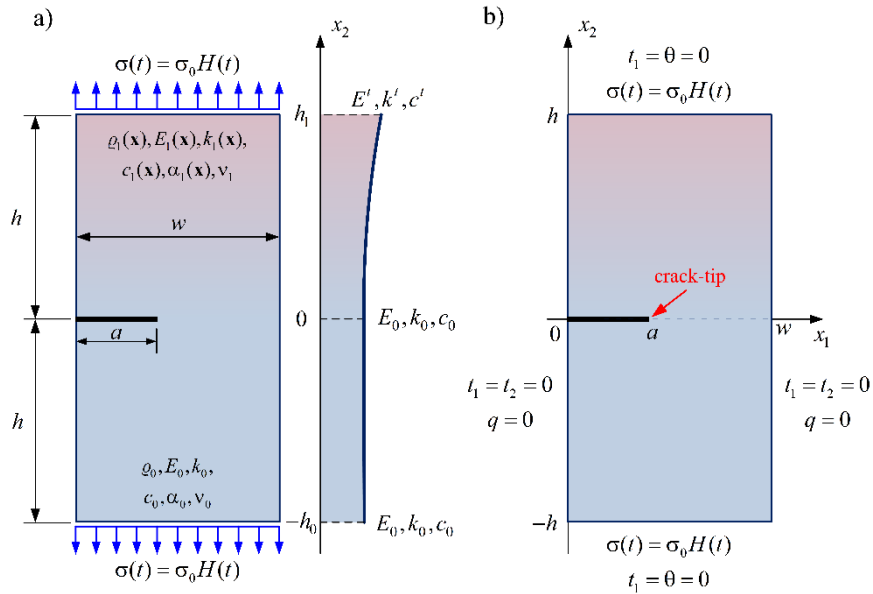


Figure 1: An edge crack in a FG/homogeneous bimaterial plate

To test the accuracy of the proposed BEM, a homogeneous cracked plate with $\alpha_g = 0$ is first considered. The normalized mode-I SIF \bar{K}_I is given in Fig. 2. The BEM result is compared to the corresponding results by Sladek et al. [11] provided by the MLPG and FEM. A very good agreement between the results is obtained, especially an excellent agreement can be observed in the time interval $t \leq 6$.

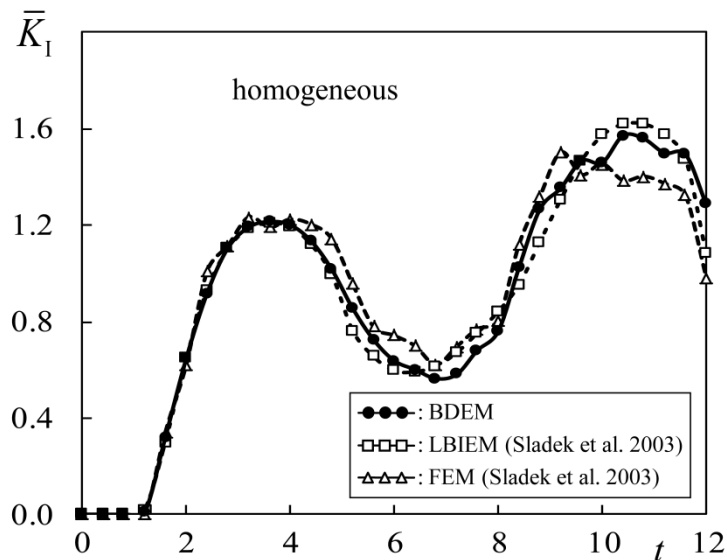


Figure 2: Normalized dynamic mode-I SIF for the homogeneous cracked plate

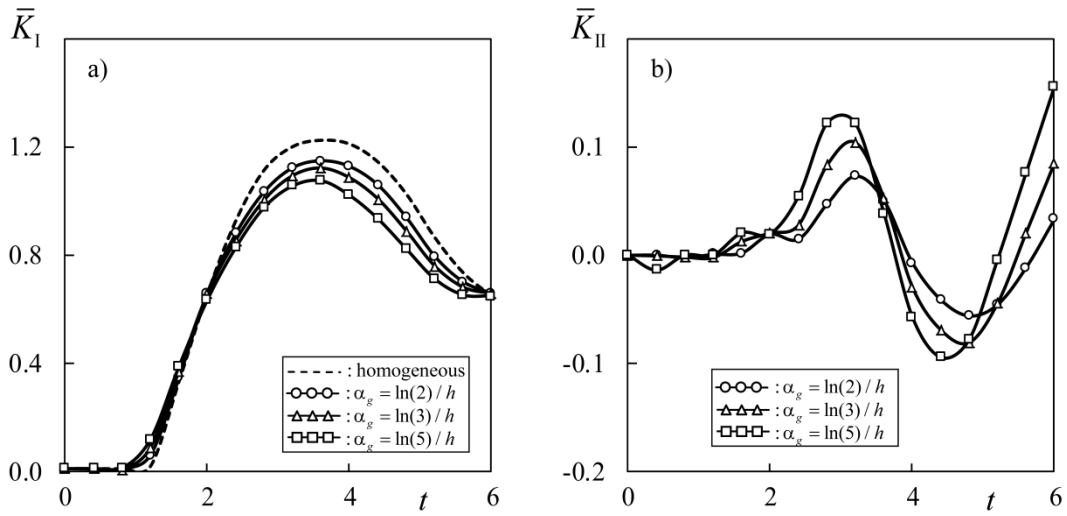


Figure 3: Normalized dynamic a) mode-I and b) mode-II SIFs for $\alpha_g h = \ln(2), \ln(3), \ln(5)$

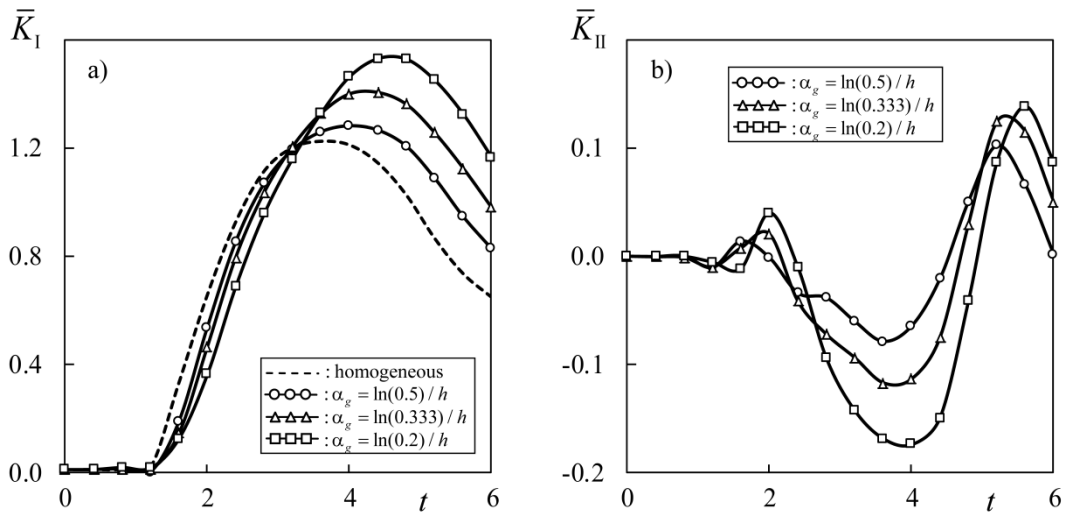


Figure 4: Normalized dynamic a) mode-I and b) mode-II SIFs for $\alpha_g h = \ln(0.5), \ln(0.333), \ln(0.2)$

To investigate the influences of the material non-homogeneity on the SIFs six material gradient parameters are selected as $\alpha_g h = \ln(2), \ln(3), \ln(5)$ and $\alpha_g h = \ln(0.5), \ln(0.333), \ln(0.2)$ in the numerical analysis. The time variations of the normalized mode-I and mode-II SIFs for the selected gradient parameters are shown in Figs. 3 and 4. The positive gradient parameters (Fig. 3) result in a reduction of the peak dynamic SIFs in comparison to that for negative gradient parameters (Fig. 4). The wave velocity in this case is also increasing. Hence, the peak values of the dynamic SIFs are reached at smaller time instants. The opposite tendency is observed in Fig. 4 with the decreasing gradient parameters. Thus, the present results show that the gradient parameters have significant influences on the

dynamic SIFs.

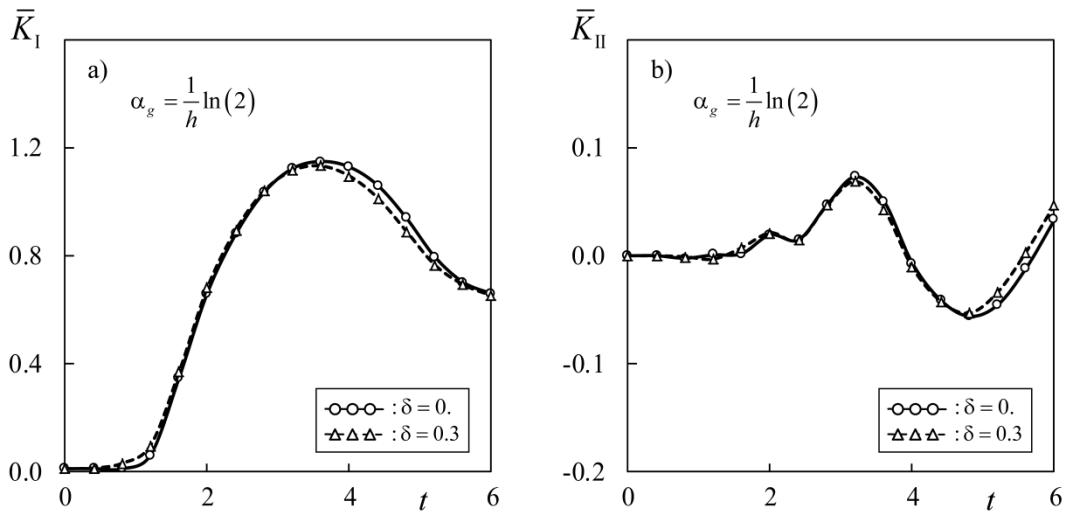


Figure 5: Normalized dynamic a) mode-I and b) mode-II SIFs for $\delta = 0, 0.3$ and $\alpha_g h = \ln(2)$

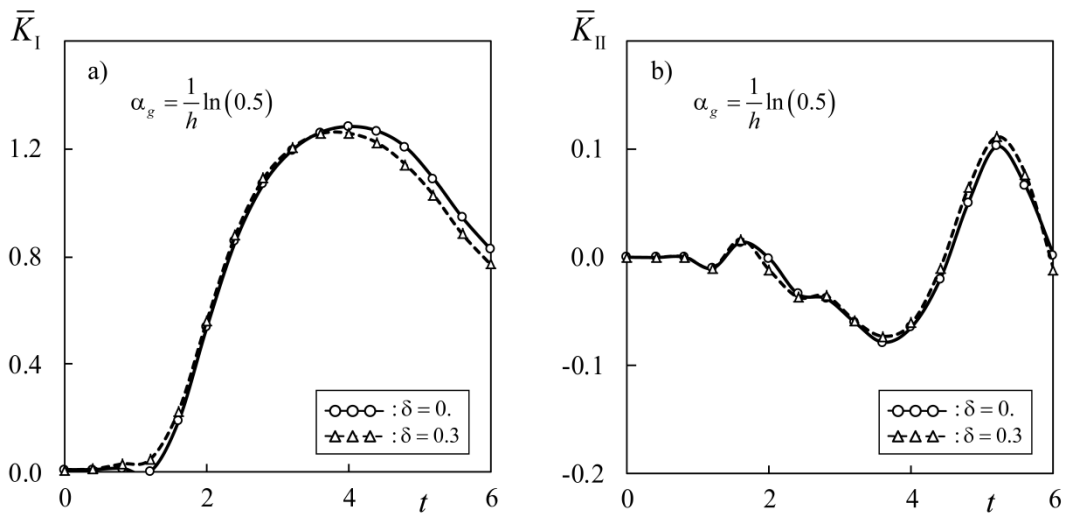


Figure 6: Normalized dynamic a) mode-I and b) mode-II SIFs for $\delta = 0, 0.3$ and $\alpha_g h = \ln(0.5)$

The effects of the thermo-mechanical coupling on the normalized dynamic mode-I and mode-II SIFs can be observed in Figs. 5 and 6. In this case, the thermo-mechanical coupling parameter (3) is taken as $\delta = 0.3$, which correspond to the previously used material parameters with the reference temperature $T_0 = 225$. With the increase of the coupling parameter, the peak values of the normalized dynamic SIFs are reduced. The numerical results imply that the influence of the thermo-mechanical coupling on the dynamic SIFs is much weaker in comparison to the influences of the material gradation.

5 SUMMARY

A 2-D transient thermoelastic crack analysis in isotropic, non-homogeneous and linear elastic FGMs subjected to impact loading is presented in this paper. For this purpose, a BEM is proposed. Fundamental solutions of linear coupled thermoelasticity for the corresponding homogeneous, isotropic and linear elastic materials in the Laplace-transformed domain are employed to derive the boundary-domain integral equation formulations. The material non-homogeneity is described by domain integrals, which are evaluated by using the RIM. A collocation-based BEM is developed in the Laplace-transformed domain. The numerical inversion of the Laplace-transform is performed by using the Stehfest's algorithm. The temporal variations of the dynamic SIFs for an edge crack in 2-D FGM plate are presented. Numerical results demonstrate that the material gradation have significant influences on the dynamic SIFs, namely their peak values and the corresponding time instants, at which they appear. On the contrary, influences of the thermo-mechanical coupling on the dynamic SIFs are much weaker in comparison to the influences of the material gradation.

Acknowledgement

This work is supported by the German Research Foundation (DFG, Project-No.: ZH 15/10-2), which is gratefully acknowledged.

REFERENCES

- [1] Suresh, S. and Mortensen, A. *Fundamentals of functionally graded materials: processing and thermomechanical behaviour of graded metals and metal-ceramic composites*. IOM Communications Ltd, (1998).
- [2] Balas, J., Sladek, J., Sladek, V. *Stress analysis by boundary element methods*. Elsevier, (1989).
- [3] Ekhlakov, A.V., Khay, O.M., Zhang, Ch., Sladek, J. and Sladek, V. Transient coupled thermoelastic crack analysis in functionally graded materials. *Struct. Durab. Health. Monitor.* (2010) **6**:329-350.
- [4] Ekhlakov, A.V., Khay, O.M., Zhang, Ch., Sladek, J. and Sladek, V. A BDEM for transient thermoelastic crack problems in functionally graded materials under thermal shock. *Comput. Mater. Sci.* (2012) **57**:30-37.
- [5] Ekhlakov, A.V., Khay, O.M., Zhang, Ch., Sladek, J. and Sladek, V. Thermoelastic crack analysis in functionally graded materials and structures by a BEM. *Fatigue & Fract. of Eng. Mater. & Struct.* (2012) **35**:742-766.
- [6] Gao, X.W. A boundary element method without internal cells for two-dimensional and three-dimensional elastoplastic problems. *J. Appl. Mech.* (2002) **69**:154-160.
- [7] Gao, X.W. The radial integration method for evaluation of domain integrals with boundary-only discretization. *Eng. Anal. Boundary Elem.* (2002) **26**:905-916.
- [8] Stehfest, H. Numerical inversion of Laplace transforms. *Commun. of the ACM* (1970) **13**:47-49.
- [9] Sladek, J., Sladek, V., Zhang, C. and Tan, C.L. Meshless local Petrov-Galerkin method for linear coupled thermoelastic analysis. *Comp. Model. Eng. Sci.* (2006) **16**:57-68.

- [10] Wrobel L.C. and Aliabadi M.H. *The boundary element method*. J. Wiley, (2002).
- [11] Sladek, J., Sladek V. and Zhang, C. An advanced numerical method for computing elastodynamic fracture parameters in functionally graded materials. *Comput. Mater. Sci.* (2005) **32**:532-543.